Eur. Phys. J. A **1**, 125–135 (1998)

**THE EUROPEAN PHYSICAL JOURNAL A**
© Springer-Verlag 1998

# High spin states and evidence for octupole correlations in $^{117}$Xe

Z. Liu[1], X. Sun[1], X. Zhou[1], X. Lei[1], Y. Guo[1], Y. Zhang[1], X. Chen[1], H. Jin[1], Y. Luo[1], S.X. Wen[2], C.X. Yang[2], G.J. Yuan[2], G.S. Li[2], X.A. Liu[2], W.D. Luo[2], Y.S. Chen[2]

[1] Institute of Modern Physics, Chinese Academy of Sciences, Lanzhou 730000, People's Republic of China
[2] China Institute of Atomic Energy, Beijing 102413, People's Republic of China

Received: 17 June 1997 / Revised version: 29 September 1997
Communicated by B. Herskind

**Abstract.** High-spin states of $^{117}$Xe were investigated by means of in-beam $\gamma-$ray spectroscopic techniques via the reaction of $^{28}$Si bombarding a $^{92}$Mo target at beam energies of 100-120 MeV. A positive-parity rotational band decaying into the yrast negative-parity band by a series of enhanced E1 transitions was observed for the first time, implying the existence of octupole correlations in $^{117}$Xe. The B(E1) values increase with spin. The $\nu d_{5/2}$ band was firmly established up to $27/2^+$ and the B(M1)/B(E2) ratios were extracted from the relative intensities of $\gamma$-rays in this band. The previously known $\nu h_{11/2}$ and $\nu g_{7/2}$ $[413]5/2^+$ $\alpha = -1/2$ bands were confirmed and extended up to high spins and two bandcrossings are observed in the latter at $\hbar\omega$=0.33 and 0.44 MeV, respectively. The bandcrossings and configurations of these bands are discussed by TRS and CSM calculations. In a $\gamma-\gamma-t$ measurement, the $11/2^-$ and $7/2^-$ levels were identified as two isomers with half-lives of 59.4±20 ns and 16.5±8.0 ns, respectively.

**PACS.** 21.10.Re Collective levels and giant resonances – 23.20.Lv Gamma transitions and level energies – 27.60.+j $90 \leq A \leq 149$

## 1 Introduction

The diversity of structure in the neutron-deficient transitional nuclei with A∼120 (53≤Z≤56) has attracted much attention in recent years. Coexistence of collective oblate shape and prolate shape [1], non-collective oblate states associated with band termination [1,2,3] and bandcrossings originating from the alignment of $h_{11/2}$ neutrons as well as $h_{11/2}$ protons [4] have been observed and compared to the theoretical calculations. A particularly interesting structural feature, which however, has not yet been well investigated in this region, is the octupole correlations. Theoretical calculations predicted the existence of octupole deformations in ground states for nuclei with both neutron and proton number close to 56, 88, 136 [5,6]. These three numbers correspond to the situations where the Fermi level lies between the intruder subshell (N+1, l, j) and the normal parity subshell (N, l-3, j-3). Manifestations of octupole deformation or strong octupole correlations have been experimentally observed in the regions of the light Ra and Th (Z≈88, N≈136), and of the heavy Ba nuclei (Z≈56, N≈88). The very light Xe and Ba isotopes with Z≈N≈56 have also been suggested as candidates for enhanced octupole collectivity on the basis of Strutinsky-type calculations [7] and of the calculations using HFBCS+GCM method [8]. These calculations show that the nuclei with Z≈N≈56 either possess a very shallow octupolly deformed minima in the Strutinsky ground-state deformation energy [7] or octupole collectivity enhanced by dynamical correlations [8]. Unfortunately, these very neutron-deficient nuclei are predicted to lie either outside the proton-drip line or very close to its border [9], and the spectroscopic information available for these nuclei are very rare. $^{114}$Xe [10] and $^{110}$Te [11] are up to now the two isotopes closest to Z=N=56, in which octupole correlations have been reported. In $^{114}$Xe, however, the B(E1) value of the $5^- \rightarrow 6^+$ transition is two orders of magnitude larger than that of the $5^- \rightarrow 4^+$, contradicting a simple interpretation based on fixed intrinsic octupole deformation. In $^{110}$Te, the observed B(E1) strengths are comparable to those in the neutron-rich barium region, but are about an order of magnitude larger than that found in $^{114}$Xe, making the Tz scaling of the dipole moment suggested in [10] questionable. Moreover, the calculations predicted that octupole softness disappear rapidly when N or Z differ from 56 by more than a few units [7]. Enhanced E1 transitions, which are considered as the most prominent experimental evidence for octupole correlations, have been observed in $^{118,120,121}$Xe isotopes recently [12,13]. These isotopes go far beyond the calculated scope of the nuclei possessing octupole softness at ground states. Therefore, more and systematic experiments are necessary to investigate whether this phenomenon is common in the Z≈56, N>60 region. Theoretical studies are also called for to explore the origin of the octupole correlations in these heavier nuclei.

We studied $^{117}$Xe in two experiments. Prior to our first experiment the excited states of $^{117}$Xe were studied by in-

beam experiments [14,15] and $^{117}$Cs decay [16]. Only the $\nu h_{11/2}$ and $\nu g_{7/2}$ bands were established and the knowledge of the excited states based on the other quasiparticle excitations was quite limited. The preliminary results of our first experiment have been presented in international workshops [17,18] and published in [19]. The second experiment provides more and important structure information. Recently the yrast band of $^{117}$Xe has been pushed up to $I^{\pi}$=$91/2^{-}$ by Paul et al. [4].

## 2 Experimental details

Excited states of $^{117}$Xe were populated by bombarding a 2mg/cm$^2$ thick isotopically enriched $^{92}$Mo (94%) target with a $^{28}$Si beam at energies of 100-120 MeV. The $^{28}$Si beam was provided by the HI-13MV tandem accelerator, Beijing. The target was supported with a 6mg/cm$^2$ lead backing to stop the recoil residual nuclei, so as to minimize the Doppler shift in the measured $\gamma$-ray energies. The $\gamma$-rays were detected by seven BGO Compton surpressed HPGe detectors placed at $\theta = \pm 28°$, 33°, 70°, 75°, 90°, 143° with respect to the beam direction. A 14 element BGO crystal ball served as a multiplicity filter and its fired fold was recorded as a parameter. Excitation functions were measured first in the energy range of 100-120 MeV with a 5 MeV step, and an optimal beam energy of 115 MeV was found, at which the $^{117}$Xe yield is dominating. Then a prompt coincidence measurement was performed with a coincidence time window of 40 ns at this beam energy in the first experiment. About 90 million $\gamma - \gamma$ coincidence events were collected and analyzed as described in [19].

The low-spin part ($j \leq 11/2$) of the $h_{11/2}$ band in light ($N < 70$) odd-A Xe isotopes is characterized by very narrow level spacings. These negative-parity low-spin states are usually isomers with half-lives in tens of nanoseconds range [20,21]. In the prompt coincidence spectra of the first measurement, the 205 keV transition was found much weaker than the 401 keV transition, indicating the existence of at least one isomer among the $7/2^{-}$ and $11/2^{-}$ states. In order to identify the isomeric states and determine their half-lives, coincidence measurements with a time window of 200 ns were performed in the second experiment, in which seven BGO Compton-suppressed HPGe detectors and one HPGe-planar detector used. A simplified delayed-coincidence electronics circuit [22] was adopted to record the absolute time difference between two coincident $\gamma-$rays. About $45\times10^6$ $\gamma - \gamma - t$ events were obtained. Only the two-fold coincidence events were selected in sorting the coincidence time spectra.

The $\gamma - \gamma - t$ coincidence events with $t \leq$40 ns were gain matched and accumulated into the $E_\gamma$-$E_\gamma$ prompt coincidence matrix obtained in the first experiment to increase the statistics. To assist in the assignment of transition multipolarities, angular correlation information was extracted from the coincidence data. The three detectors close to $\theta = 90°$ were sorted against the other four forward and backward detectors and the average directional correlation (DCO) ratios [23] were extracted. The obtained DCO ratios for the known stretched E2 ($\Delta I = 2$) and stretched dipole ($\Delta I = 1$) transitions are about unity (0.8∼1.1) and 0.5 (0.4∼0.7), respectively, when gated on E2 transitions.

Gamma-ray angular distributions were also measured by using a simple and time saving procedure. Six BGO-suppressed HPGe detectors were simultaneously placed at $\theta = 20°$, 39°, 55°, 75°, 90° and 145° with respect to the beam direction, respectively, to record $\gamma$ singles. The in-beam relative detection efficiency curves for these detectors are crucial for deducing the relative $\gamma-$ray intensities at each angle. For a specific detector, the in-beam and the off-beam relative detection efficiencies vary by the ratio of the in-beam dead time correction factor to the off-beam one. This ratio was measured by inputting signals of the precise pulse generator into the preamplifiers of the HPGe detectors. The off-beam relative detection efficiency curves were obtained by measuring the isotropic residual radioactivity from the target off-beam. The normalized $\gamma-$ray intensities at each angle were fitted to the standard Legendre expansion

$$W(\theta) = A_0 + A_2 P_2(\cos\theta) + A_4 P_4(\cos\theta) \qquad (1)$$

to extract the $A_2/A_0$, $A_4/A_0$ angular distribution coefficients.

## 3 The level scheme

In the present study, the combination of $^{28}$Si projectiles of 115 MeV and a $^{92}$Mo target favors the absolute and relative population of $^{117}$Xe. The resulting $^{117}$Xe level scheme is presented in Fig. 1. Assignments of the new $\gamma$-rays to $^{117}$Xe are from the connections with the known $\gamma$-rays. The placement of the $\gamma$-ray transitions is based on the coincidence relationships and their relative intensities. The spins and parities of the levels are determined mainly on the basis of the measured angular distributions and the DCO ratios. The transition energies, intensities and the assignments of the $\gamma$ rays are listed in Table 1 together with the derived angular-distribution-coefficient ratios and their DCO information.

Bands 2 and 1 are the favored and unfavored signatures of the unique parity $\nu h_{11/2}$ band, respectively, first were observed by Chowdhury et al. [14]. In the present study, the observation of the 107 keV $\gamma-$ray in coincidence with the 205 and 386 keV transitions, together with the identification of the two isomers (see Sect. 4) between the 401 and 205 keV transitions confirmed the bottom part of the $h_{11/2}$ band proposed by Törmänen et al. [12]. Band 2 is definitely established up to $39/2^{-}$. A weak 990 keV transition which was not observed in [12] was found to be in coincidence with the lower transitions in this band. Recently, this band has been greatly augmented to $(91/2^{-})$ using the Eurogam II spectrometer [4]. The 794 and 802 keV transitions were found in coincidence with the known transitions of band 1 and show stretched quadrupole (E2) character (with DCO ratios of 0.71 and 0.84, respectively).

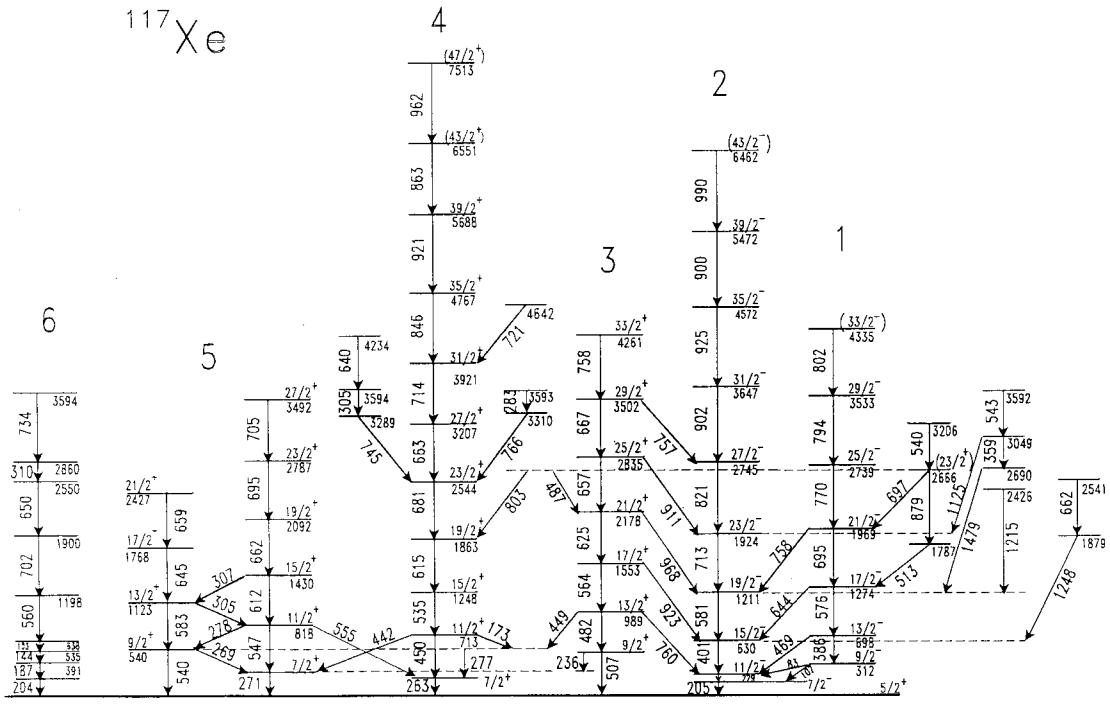


**Fig. 1.** Level scheme proposed for $^{117}$Xe by present work

This unfavored signature band is extended up to $(33/2^-)$ tentatively.

Band 3 is established first in the present work. It consists of a series of stretched E2 transitions built on the 507 keV level. Its remarkable feature is that it decays out to the yrast band (band 2) via five distinct transitions, the intraband and the interband transitions are clearly seen in the gated coincidence spectra shown in Fig. 2. This band also decays directly to the ground state through the 236 and 271 keV cascade or the 507 keV crossover transition. The DCO ratios of the 236 and 507 keV transitions are consistent with stretched dipole ($\Delta$I=1) and quadrupole ($\Delta$I=2), respectively. Intensity balance considerations (the intensity of the 507 keV is stronger than that of the 236 keV transition) favor the assignments of M1(E2) and E2 to the 236 keV and the 507 keV transitions, respectively. Therefore, the 507 keV level, the bandhead of band 3, has the $j^\pi = 9/2^+$ and band 3 is a positive-parity band. This assignment is supported by the E2 character of the 449 keV transition (with DCO ratio of 0.93), which occurs between the 989 keV $13/2^+$ level of band 3 and the 540 keV $9/2^+$ state of band 5. Hence, the interband transitions between band 3 and band 2 are stretched dipole E1 transitions, in agreement with their DCO ratios and the angular distribution measured for the 968 keV transition. This band was established up to $33/2^+$ and tentatively assigned as the $\nu g_{7/2}$ $\alpha$=+1/2 band in our previous paper [19].

Band 4 is the $\nu g_{7/2}$ $\alpha = -1/2$ band first observed up to $27/2^+$ by Törmänen et al. [15]. Five new transitions (714, 846, 921, 863 and 962 keV) are coincident with the lower transitions. Their DCO ratios manifest that they are stretched quadrupole (E2) transitions. Several other $\gamma$ lines, such as the 721, 745 and 766 keV transitions, are observed feeding the band at $23/2^+$and $31/2^+$, respectively, establishing some new levels. Some of these new transitions were also reported in [12], but the 745 keV line was placed differently.

Band 5 is the third positive-parity band, involving two signatures linked by M1 transitions. It appears to be directly built on the ground state. The $\alpha = -1/2$ signature branch of this band was established up to $27/2^+$ in the first experiment [19]. After our first round experiment this band was reported by Törmänen et al. [12] up to $(15/2^+)$ and $(17/2^+)$ for the $\alpha = -1/2$ and $\alpha = +1/2$ signatures, respectively. Thanks to the statistically improved data, we were able to identify the $\alpha = +1/2$ branch and to extract the B(M1)/B(E2) values (see Sect. 5.4).

A 540 keV transition is observed coincident with all of the lower lying transitions in bands 1, 2, 3 and 4. The DCO ratio (0.87) of the most intensive 803 keV linking transition favors a stretched quadrupole, establishing a tentative $23/2^+$ level at 2666 keV, which decays to band 1, 3 and 4 through different paths. Several high energy transitions (1248, 1215, 1479 and 1125 keV) are observed feeding the yrast band (band 2) at $15/2^-$, $19/2^-$ and $23/2^-$, respectively.

In the present study some new transitions were found to be in coincidence with the 204, 187, 144 keV cascade identified in the decay of $^{117}$Cs [16]. They are arranged into a level sequence of band 6 in Fig. 1 according to their relative intensities and coincidence relationships. This level

**Table 1.** The $\gamma$-ray energies, relative intensities, DCO ratios and angular distributions for transitions assigned to $^{117}$Xe following the reaction $^{92}$Mo($^{28}$Si, 2pn)$^{117}$Xe at 115 MeV

| $E_\gamma$ [a] (keV) | $I_\gamma$ [b] | DCO ratios | $A_2/A_0$ | $A_4/A_0$ | Band | Assignment |
|---|---|---|---|---|---|---|
| 83.4 | 40.8 [d] | 0.74 | | | 1→2 | $\frac{9}{2}^- \rightarrow \frac{11}{2}^-$ |
| 102.5 | | | | | 6 | |
| 107.0 | | 0.56 | | | 1→2 | $\frac{9}{2}^- \rightarrow \frac{7}{2}^-$ |
| 385.8 | 14.7 | 1.14 | | | 1 | $\frac{13}{2}^- \rightarrow \frac{9}{2}^-$ |
| 144.0 | | | | | 6 | |
| 173.0 | [d] | 0.49 | | | 4→5 | $\frac{11}{2}^+ \rightarrow \frac{9}{2}^+$ |
| 187.0 | | | | | 6 | |
| 204.0 | | | | | 6 | |
| 205.0 | 98.0(7) [c,d] | 0.56 | -0.20 | 0.07 | 2 | $\frac{7}{2}^- \rightarrow \frac{5}{2}^+$ |
| 236.0 | 3.1 | 0.57 | | | 3 | $\frac{9}{2}^+ \rightarrow \frac{7}{2}^+$ |
| 262.9 | 22.8(5)[c,d] | 0.43 | -0.46 | 0.13 | 4 | $\frac{7}{2}^+ \rightarrow \frac{5}{2}^+$ |
| 268.5 | 6.0 | 0.58 | | | 5 | $\frac{9}{2}^+ \rightarrow \frac{7}{2}^+$ |
| 271.0 | 20.9(4) [c,d] | 0.24 | -0.57 | 0.11 | 5 | $\frac{7}{2}^+ \rightarrow \frac{5}{2}^+$ |
| 276.9 | [d] | 0.63 | | | 5→4 | $\frac{9}{2}^+ \rightarrow \frac{7}{2}^+$ |
| 277.8 | [d] | 1.03 | | | 5 | $\frac{11}{2}^+ \rightarrow \frac{7}{2}^+$ |
| 283.4 | 1.0 | | | | | |
| 304.6 | 2.2 | | | | →4 | $\rightarrow \frac{23}{2}^+$ |
| 305.0 | 2.7 | 0.38 | | | 5 | $\frac{13}{2}^+ \rightarrow \frac{11}{2}^+$ |
| 307.4 | 1.0 | | | | 5 | $\frac{15}{2}^+ \rightarrow \frac{13}{2}^+$ |
| 309.6 | | | | | 6 | |
| 358.5 | 1.6 | | | | | |
| 385.8 | 14.7 | 1.14 | | | 1 | $\frac{13}{2}^- \rightarrow \frac{9}{2}^-$ |
| 400.7 | 100.0(4) [c] | 1.04 | 0.26 | -0.04 | 2 | $\frac{11}{2}^- \rightarrow \frac{7}{2}^-$ |
| 442.0 | 12.6 | 1.01 | 0.30 | -0.02 | 4→5 | $\frac{11}{2}^+ \rightarrow \frac{7}{2}^+$ |
| 449.0 | [d] | 0.93 | | | 3→5 | $\frac{13}{2}^+ \rightarrow \frac{9}{2}^+$ |
| 450.0 | 28.1 | 1.02 | | | 4 | $\frac{11}{2}^+ \rightarrow \frac{7}{2}^+$ |
| 469.4 | 9.8 | 0.26 | | | 1→2 | $\frac{13}{2}^- \rightarrow \frac{11}{2}^-$ |
| 481.7 | 8.9(3) [c] | 0.95 | 0.28 | -0.03 | 3 | $\frac{13}{2}^+ \rightarrow \frac{9}{2}^+$ |
| 487.0 | | | | | →3 | $(\frac{23}{2}^+) \rightarrow \frac{21}{2}^+$ |
| 507.0 | 6.7 | 0.90 | | | 3 | $\frac{9}{2}^+ \rightarrow \frac{5}{2}^+$ |
| 513 | 2.6 [d] | | | | →1 | $\rightarrow \frac{17}{2}^-$ |
| 534.9 | 36.0 | 1.03 | 0.16 | 0.01 | 4 | $\frac{15}{2}^+ \rightarrow \frac{11}{2}^+$ |
| 539.8 | [d] | 0.96 | | | 5 | $\frac{9}{2}^+ \rightarrow \frac{5}{2}^+$ |
| 540.0 | 6.7(2)[c,d] | | | | →1,3,4 | $\rightarrow (\frac{23}{2}^+)$ |
| 543.0 | 4.3 | 0.85 | | | | |
| 546.7 | 5.6 | 0.93 | | | 5 | $\frac{11}{2}^+ \rightarrow \frac{7}{2}^+$ |
| 554.7 | 3.2 | | | | 5→4 | $\frac{11}{2}^+ \rightarrow \frac{7}{2}^+$ |
| 560.1 | | | | | 6 | |
| 564.3 | 9.3 | 0.96 | | | 3 | $\frac{17}{2}^+ \rightarrow \frac{13}{2}^+$ |
| 575.9 | 22.6 | 1.02 | | | 1 | $\frac{17}{2}^- \rightarrow \frac{13}{2}^-$ |
| 580.9 | 70.1 | 1.01 | 0.27 | -0.05 | 2 | $\frac{19}{2}^- \rightarrow \frac{15}{2}^-$ |
| 583.0 | 4.1 | 0.90 | | | 5 | $\frac{13}{2}^+ \rightarrow \frac{9}{2}^+$ |
| 612.1 | 8.3 | 0.79 | | | 5 | $\frac{15}{2}^+ \rightarrow \frac{11}{2}^+$ |
| 615.1 | 34.2(5) [c] | 0.95 | 0.24 | 0.00 | 4 | $\frac{19}{2}^+ \rightarrow \frac{15}{2}^+$ |
| 625.4 | 9.2 | 0.90 | | | 3 | $\frac{21}{2}^+ \rightarrow \frac{17}{2}^+$ |
| 639.7 | 1.7 | | | | →4 | $\rightarrow \frac{23}{2}^+$ |
| 644.5 | 5.4 | 0.39 | | | 1→2 | $\frac{17}{2}^- \rightarrow \frac{15}{2}^-$ |
| 645.4 | 3.7 | 1.08 | | | 5 | $\frac{17}{2}^+ \rightarrow \frac{13}{2}^+$ |
| 650.0 | | | | | 6 | |
| 656.7 | 4.3 | 1.06 | | | 3 | $\frac{25}{2}^+ \rightarrow \frac{21}{2}^+$ |

**Table 1.** contd.

| $E_\gamma$ [a] (keV) | $I_\gamma$ [b] | DCO ratios | $A_2/A_0$ | $A_4/A_0$ | Band | Assignment |
|---|---|---|---|---|---|---|
| 659.0 | [d] | 0.85 | | | 5 | $\frac{21}{2}^+ \rightarrow \frac{17}{2}^+$ |
| 662.0 | [d] | | | | | |
| 662.1 | 16.0 [d] | 1.26 | | | 5 | $\frac{19}{2}^+ \rightarrow \frac{15}{2}^+$ |
| 663.0 | 9.0 | 0.94 | | | 4 | $\frac{27}{2}^+ \rightarrow \frac{23}{2}^+$ |
| 667.4 | 2.1 | 0.83 | 0.40 | -0.02 | 3 | $\frac{29}{2}^+ \rightarrow \frac{25}{2}^+$ |
| 681.0 | 26.3 | 0.99 | | | 4 | $\frac{23}{2}^+ \rightarrow \frac{19}{2}^+$ |
| 695.0 | 5.3 | 0.72 | | | 5 | $\frac{23}{2}^+ \rightarrow \frac{19}{2}^+$ |
| 695.1 | 17.2 | 0.94 | | | 1 | $\frac{21}{2}^- \rightarrow \frac{17}{2}^-$ |
| 702.0 | | | | | 6 | |
| 704.6 | 3.2 | 0.80 | | | 5 | $\frac{27}{2}^+ \rightarrow \frac{23}{2}^+$ |
| 713.0 | 45.9 | 0.95 | 0.25 | 0.02 | 2 | $\frac{23}{2}^- \rightarrow \frac{19}{2}^-$ |
| 713.6 | 9.1 | 0.74 | | | 4 | $\frac{31}{2}^+ \rightarrow \frac{27}{2}^+$ |
| 721.4 | 2.2 | | | | →4 | $\rightarrow \frac{31}{2}^+$ |
| 734.4 | | | | | 6 | |
| 745.1 | 6.9 | | | | →4 | $\rightarrow \frac{23}{2}^+$ |
| 757.3 | $\leq 1.0$[d] | 0.75 | | | 3 → 2 | $\frac{29}{2}^+ \rightarrow \frac{27}{2}^-$ |
| 758 | 1.0 | 0.85 | | | 3 | $\frac{33}{2}^+ \rightarrow \frac{29}{2}^+$ |
| 758.3 | 3.4 | | | | 1→2 | $\frac{21}{2}^- \rightarrow \frac{19}{2}^-$ |
| 759.7 | 5.0 | 0.61 | | | 3→2 | $\frac{13}{2}^+ \rightarrow \frac{11}{2}^-$ |
| 766.1 | 6.7 | | | | →4 | $\rightarrow \frac{23}{2}^+$ |
| 769.7 | 10.1 | 0.88 | | | 1 | $\frac{25}{2}^- \rightarrow \frac{21}{2}^-$ |
| 793.6 | 5.2 | 0.71 | | | 1 | $\frac{29}{2}^- \rightarrow \frac{25}{2}^-$ |
| 802.1 | 2.4 | 0.84 | | | 1 | $(\frac{33}{2}^-) \rightarrow \frac{29}{2}^-$ |
| 803.4 | 3.9 | 0.87 | | | →4 | $(\frac{23}{2}^+) \rightarrow \frac{19}{2}^+$ |
| 820.5 | 21.5 | 0.80 | 0.12 | -0.01 | 2 | $\frac{27}{2}^- \rightarrow \frac{23}{2}^-$ |
| 846.5 | 1.4 | 0.79 | | | 4 | $\frac{35}{2}^+ \rightarrow \frac{31}{2}^+$ |
| 863.0 | $\leq 1.0$ | 0.96 | | | 4 | $(\frac{43}{2}^+) \rightarrow \frac{39}{2}^+$ |
| 879.3 | 3.0 | | | | 1→2 | $\frac{9}{2}^- \rightarrow \frac{11}{2}^-$ |
| 899.8 | 4.0 | 0.74 | | | 2 | $\frac{39}{2}^- \rightarrow \frac{35}{2}^-$ |
| 902.3 | 10.3 | 0.75 | | | 2 | $\frac{31}{2}^- \rightarrow \frac{27}{2}^-$ |
| 911.2 | 2.3 | 0.64 | | | 3→2 | $\frac{25}{2}^+ \rightarrow \frac{23}{2}^-$ |
| 921.0 | 1.0 | 1.04 | | | 4 | $\frac{39}{2}^+ \rightarrow \frac{35}{2}^+$ |
| 923.4 | 5.1 | 0.35 | | | 3→2 | $\frac{17}{2}^+ \rightarrow \frac{15}{2}^-$ |
| 924.7 | 4.5 | 0.68 | 0.10 | -0.03 | 2 | $\frac{35}{2}^- \rightarrow \frac{31}{2}^-$ |
| 961.6 | $\leq 1.0$ | 0.94 | | | 4 | $(\frac{47}{2}^+) \rightarrow (\frac{43}{2}^+)$ |
| 967.7 | 5.2 | 0.57 | -0.36 | 0.00 | 3→2 | $\frac{21}{2}^+ \rightarrow \frac{19}{2}^-$ |
| 990.0 | 1.8 | | | | 2 | $(\frac{43}{2}^-) \rightarrow \frac{39}{2}^-$ |
| 1125.0 | 2.6 | | | | →2 | $\rightarrow \frac{23}{2}^-$ |
| 1215.1 | 1.9 | | | | →2 | $\rightarrow \frac{19}{2}^-$ |
| 1247.9 | 1.4 | 0.36 | 0.09 | 1.41 | →2 | $\rightarrow \frac{15}{2}^-$ |
| 1479.4 | 2.2 | | | | →2 | $\rightarrow \frac{19}{2}^-$ |

a: $\gamma$-ray energies are accurate to $\pm$0.5 keV, except those quoted as integers which are accurate to $\pm$1.0 keV.
b: Transition intensities were obtained from a combination of singles and coincidence data and are normalized to the 400.7 keV $\frac{11}{2}^- \rightarrow \frac{7}{2}^-$ transition. The quoted values have been corrected for detector efficiency. Typical erros are estimated to be less than 15%.
c: Intensities were obtained from single spectra.
d: Disturbed by other $\gamma$-rays with very close energy produced in the same reaction.

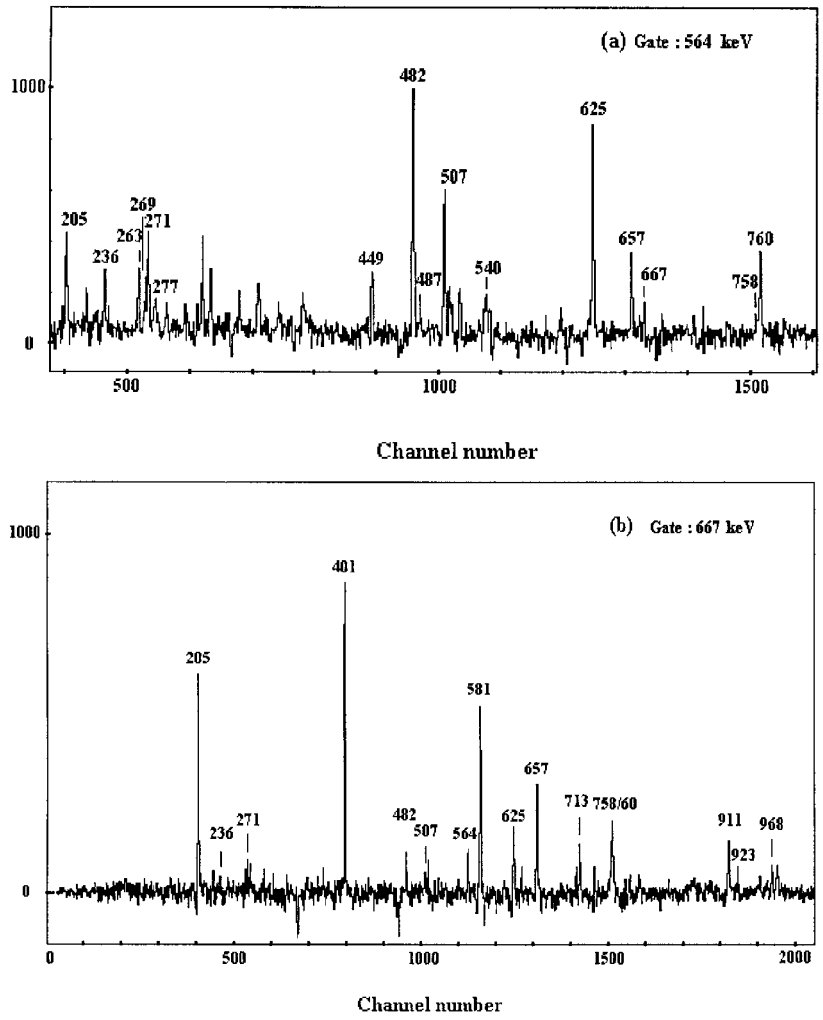


**Fig. 2.** Typical coincidence spectra gated on **a** 564 keV and **b** 667 keV transitions in band 3

sequence is characterized by its irregular level spacings. Spins and parities were not suggested for these levels since the angular distribution and DCO information could not be extracted for these transitions.

## 4 Determination of isomer half-lives

Due to the low energy and the large electron conversion coefficient for the 24 keV ($11/2^- \rightarrow 7/2^-$) E2 transition, it was not observed even in the HPGe planar detector. Because of the weakness of the 107 keV transition, the half-life of the $7/2^-$ state could not be directly obtained from the coincidence time spectrum between the 107 and 205 keV transitions either. The coincidence time spectrum between the 205 and 401 keV transitions was sorted and is shown in Fig. 3. The related background has already been subtracted.

In standard delayed-coincidence measurement the relative time difference $t_d$ between two $\gamma$ rays has a distribution $F(t_d)$:

$$F(t_d) = \int_0^\infty f(t)P(t_d - t)dt \qquad (2)$$

$P(t_d)$ is the prompt-coincidence curve. f(t) is the theoretical distribution of the time difference between two coincident $\gamma$ rays, which is a function of the half-lives of the states between the two $\gamma$ rays. In our experiment the absolute time difference $|t_d|$ was recorded. Its distribution $Y(|t_d|)$ was obtained by adding $F(|t_d|)$ and $F(-|t_d|)$ together:

$$Y(|t_d|) = F(|t_d|) + F(-|t_d|)$$
$$= \int_0^\infty f(t)[P(|t_d| - t) + P(-|t_d| - t)]dt \qquad (3)$$

In Fig. 3 the time spectrum between the 401 and 205 keV transitions shows the behavior corresponding to the presence of two isomers in cascade. Therefore the following form was used for f(t):

$$f(t) = A\frac{\lambda_1\lambda_2}{\lambda_1 - \lambda_2}(e^{-\lambda_1 t} - e^{-\lambda_2 t}) \qquad (4)$$

Two half-lives of $59.4 \pm 20$ ns and $16.5 \pm 8.0$ ns were obtained from the fit and the fitted curve is also plotted in Fig. 3.

Comparing with $^{119}$Xe [20] and assuming a similar reduced E2 transition rate for the $11/2^- \rightarrow 7/2^-$ transi-

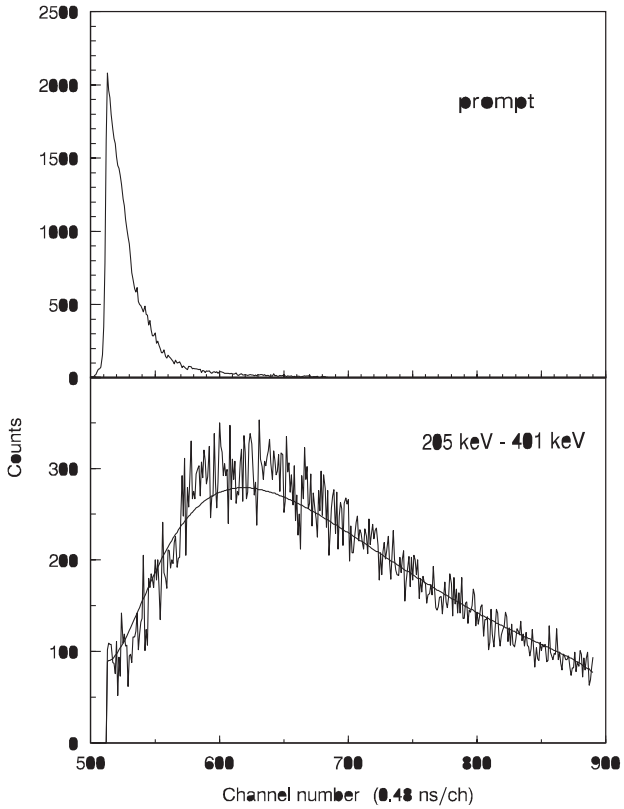


**Fig. 3.** The time spectrum between the 401 and 205 keV transitions (below), and the prompt-coincidence time ditribution curve (upper). The time distribution of the related background has been subtracted

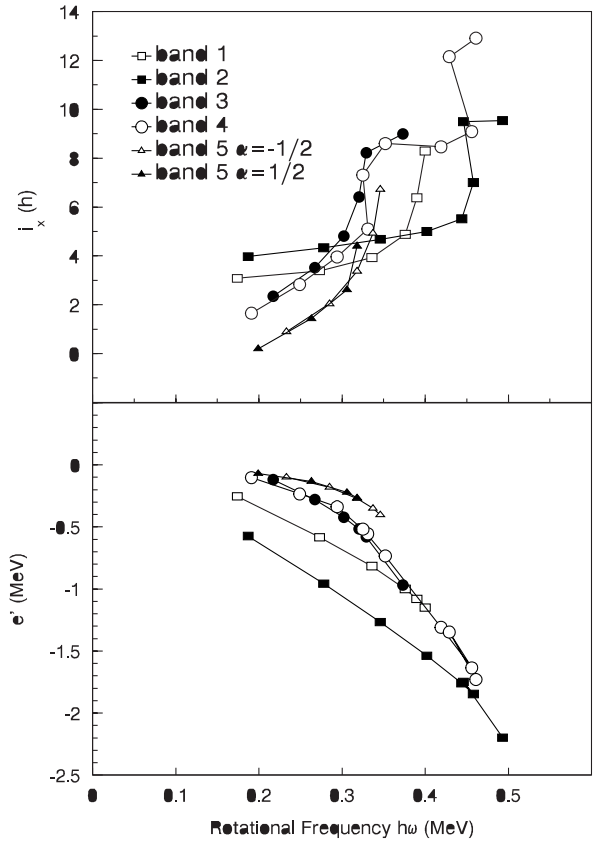


**Fig. 4.** The experimental quasiparticle alignments **a** and Routhians **b** vs rotational frequency for bands 1, 2, 3, 4, and 5 in $^{117}$Xe. A reference with Harris parameters $J_0 = 12\ \hbar^2 MeV^{-1}$ and $J_1 = 45\ \hbar^4 MeV^{-3}$ has been subtracted (see the text)

tion, a half-life of about 75 ns is expected for the $11/2^-$ state in $^{117}$Xe. So it is reasonable to assign the longer half-life of $T_{1/2}$=59.4 ns to the $11/2^-$ state, and subsequently the 16.5 ns to the $7/2^-$ state. In Törmänen et al.'s experiment [12], the stopper was 4 cm from the target down stream, and only the flight component of 205 keV $\gamma$ ray was observed in the spectrum gated on the 107 keV ($9/2^- \rightarrow 7/2^-$) transition. Using the above lifetime assignments, the stopped component is estimated to be only one tenth of the flight component for the 205 keV transition in the 107 keV gated spectrum, and is weaker than the bacground. So our result is in agreement with their observation. In order to test the reliability of the present method, we also determined the half-life for the known $9/2^+$ isomer in $^{117}$I, which was also strongly populated in the present reaction. A value of $T_{1/2}$=13.2±3.2 ns was extracted. And it is very close to the value of 12.1±1.0 ns obtained by using the pulsed-beam method [24], proving the success of the present $\gamma - \gamma - t$ experiment.

The reduced probability of a transition is sensitive to the structures of its initial and final states. With the measured half-life $T_{1/2}$=59.4 ns and the total conversion coefficient $\alpha_T \approx 520$, one has B(E2)≈0.25 $e^2b^2$ for the $11/2^- \rightarrow 7/2^-$ transition. It is very close to the B(E2) values (about 0.3 $e^2b^2$ estimated from expression (6)) of the prompt E2 transitions in the yrast $h_{11/2}$ band. This indicates that the intrinsic configurations of the low lying $11/2^-$ and $7/2^-$ states are similar to those of the higher levels in this band and that the existence of the $11/2^-$ isomer is just due to their very narrow level space. The B(E1) of the $7/2^- \rightarrow 5/2^+$ transition has been extracted to be $2.0\times10^{-6}$ W.u.. This is a normal E1 transition. The transition probabilities of the corresponding $11/2^- \rightarrow 7/2^-$ and $7/2^- \rightarrow 5/2^+$ transitions in $^{117}$Xe and $^{119}$Xe [20, 22] are close to one another, supporting that the involved level structures in these two isotopes are similar.

## 5 Discussion

In order to discuss the structures of the observed rotational bands, the experimental routhians (e') and aligned angular momenta $i_x$ of bands 1, 2, 3, 4, 5 were extracted according to [25] and are plotted as a function of rotational frequency in Fig. 4. To facilitate the comparison with the results of $^{119}$Xe, a rotational reference with Harris parameters $J_0 = 12\ \hbar^2 MeV^{-1}$ and $J1 = 45\ \hbar^4 MeV^{-3}$, obtained for $^{119}$Xe in [26], was adopted.

In order to interpret the experimental data, cranking shell model (CSM) and total routhian surface (TRS)

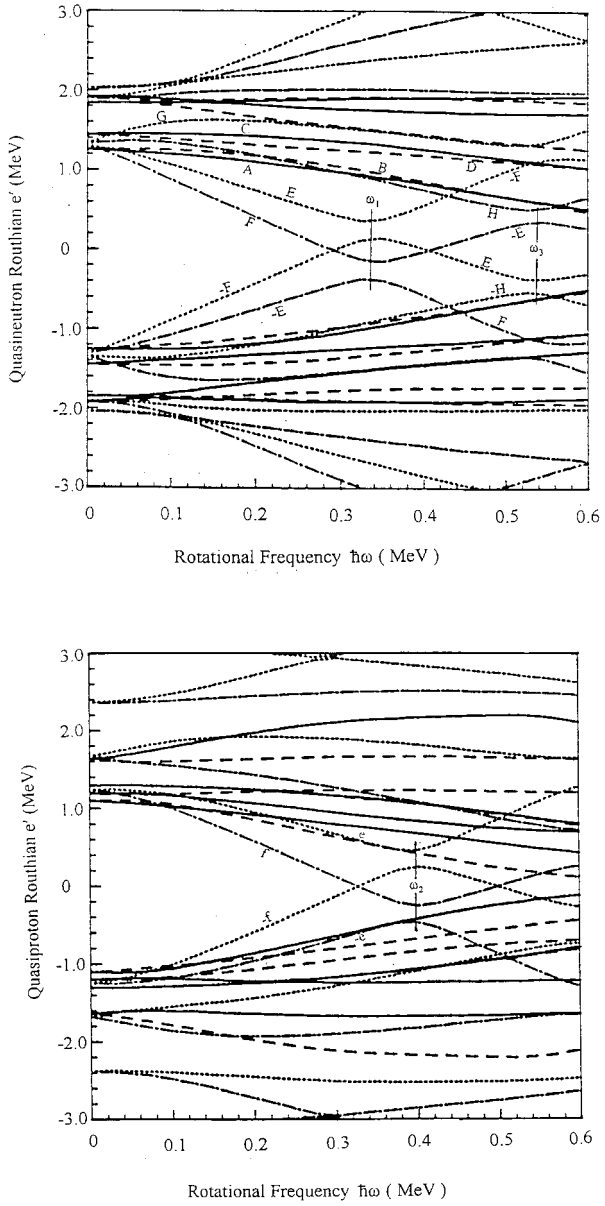


**Fig. 5.** The cranked-shell model quasiparticle Routhians for **a** neutrons calculated with the shape parameters $\beta_2 = 0.239, \gamma = -17°, \beta_4 = -0.04$ predicted for the configuration A in TRS calculations, and **b** protons calculated with shape parameters for the configuration E, $\beta_2 = 0.231, \gamma = -10°, \beta_4 = -0.04$. Pairing values were $\Delta_p = 1.10$ MeV and $\Delta_n = 1.25 MeV$. The various parity ($\pi$) and signature ($\alpha$) combinations are ($\pi$,$\alpha$)=($-$,$-\frac{1}{2}$), *dot dashed*; ($-$,$+\frac{1}{2}$), *dotted*; ($+$,$-\frac{1}{2}$), *solid*; ($+$,$+\frac{1}{2}$), *dashed*. Band crossing frequencies have been marked corresponding to the alignment of the lowest $h_{11/2}$ quasineutron ($\omega_1$), second-lowest $h_{11/2}$ quasineutron ($\omega_3$), and lowest $h_{11/2}$ quasiproton ($\omega_2$) pair

calculations have been performed for $^{117}$Xe. In the CSM calculations the deformation parameters extracted in the TRS calculations were inputted and the pairing gaps were set to $\Delta_p = 1.10$ MeV and $\Delta_n = 1.25$ MeV. As examples of the CSM calculations the quasineutron routhians calculated with the shape parameters predicted for the configuration $(+, -1/2)$ (quasiparticle A) and the quasiproton routhians calculated with the shape parameters for the configuration $(-, +1/2)$ (quasiparticle E) are plotted in Figs. 5a and 5b, respectively.

The lowest-energy, negative-parity quasiparticles correspond to the unique-parity intruder $h_{11/2}$ orbitals. K=5/2, or 3/2 is expected for neutrons (E, F, G, H), while K=1/2 is expected for protons (e,f). The lowest-energy, positive-parity quasiparticles may involve more complex single-particle structures. At the deformation of $\beta \approx 0.23, \gamma = 0°$ and $\hbar\omega = 0$, $[413]5/2^+$ ($\nu g_{7/2}$) and $[411]3/2^+$ ($\nu d_{5/2}$) are the positive-parity orbitals closest to the neutron Fermi surface in $^{117}$Xe, while the $[402]5/2^+$ ($\nu d_{5/2}$) and $[411]1/2^+$ ($\nu d_{3/2}$) orbitals are slightly further away.

### 5.1 The $\nu h_{11/2}$ band

Bands 2 and 1 represent the favored (F) and unfavored (E) signature members of the $\nu h_{11/2}$ structure, respectively. The calculations show that the $[532]5/2^-$ orbital is slightly closer to the Fermi surface than the $[541]3/2^-$ orbital at $\hbar\omega = 0$ MeV. The initial alignments of $4\hbar$ and $3\hbar$ for bands 1 and 2 are very similar to those observed in $^{119}$Xe, indicating a similar $[532]5/2^-$ nature for the $\nu h_{11/2}$ structure, at least at low rotational frequencies. The aligned angular momentum curve of band 2 experiences a sharp upbend at $\hbar\omega = 0.45$ MeV. Band 1 was pushed two levels higher and a sharp gain in the angular alignment appears at the highest two transitions, indicating that its bandcrossing frequency is around $\hbar\omega = 0.41$ MeV. Due to the blocking effect the bandcrossings in these two bands are the result of the alignment of the $h_{11/2}$ proton pair or of the lowest non-blocked $h_{11/2}$ neutron pair. At low rotational frequencies the TRS calculations give a shape of $\beta_2 = 0.229, \gamma = -18°$ for the favored ($\alpha = -1/2$) signature and $\beta_2 = 0.231, \gamma = -10°$ for the unfavored ($\alpha = 1/2$) signature. With the above calculated deformations the CSM calculations predict the proton (ef) alignment at $\hbar\omega = 0.40$ MeV for the $\alpha = 1/2$ branch (Fig. 5b) and $\hbar\omega = 0.45$ MeV for the $\alpha = -1/2$ branch, in good agreement with the experimental results, while the neutron FG alignment in the unfavored signature as well as the EH alignment in the favored signature appear at larger rotational frequencies. After this bandcrossing band 2 becomes a 3-quasiparticle configuration of $(\nu h_{11/2})(\pi h_{11/2})^2$. Lying at the bottom of the $\pi h_{11/2}$ subshell, the aligned ef quasiprotons are expected to drive the nucleus to $\gamma > 0°$ and a larger $\beta_2$. The TRS calculations predict a deformation of $\beta_2 = 0.246, \gamma = -2°$ for band 2 just after the bandcrossing.

### 5.2 Band 4

In [15] band 4 was assigned as the $\alpha = -1/2$ signature of a band built up from the $g_{7/2}$ $[413]5/2^+$ neutron state. This assignment corresponds to the A quasiparticle state

in the calculations. The aligned angular momenta are almost identical for band 4 and the favored signature of the $\nu g_{7/2}$ band in $^{119}$Xe in their overlap region, supporting the above assignment. Two bandcrossings are observed in band 4. The first one, as observed in neighboring $^{119,121}$Xe, takes place at $\hbar\omega = 0.33$ MeV. This is attributed to the alignment of the lowest pair of $h_{11/2}$ neutrons. With the calculated deformations for the A configuration, i.e., $\beta_2 = 0.239, \gamma = -17°$, the crossing frequency were well reproduced by the present CSM calculations (Fig. 5a). After the alignment of a pair of $h_{11/2}$ neutrons, the configuration of band 4 becomes AEF, of a $(\nu g_{7/2})(\nu h_{11/2})^2$ nature with a smaller deformation of $\beta_2 = 0.219, \gamma = -15°$. The second backbend is observed at $\hbar\omega = 0.44$ MeV, very close to the bandcrossing frequency observed in band 2. The CSM calculations suggest the alignment of a pair of $h_{11/2}$ protons (ef) at this frequency using the shape parameters of the AEF configuration. Thus, at the top this band becomes a five quasiparticle configuration, i.e., AEFef with a more elongated shape.

### 5.3 Band 3 – evidence for octupole correlations

Band 3 is a new positive-parity band. Its experimental routhian and aligned angular momentum curves close to those of band 4, this band looks like the signature partner of band 4 [19]. However, the statistically improved data confirmed the following unusual features of band 3: a) no transitions connecting bands 3 and 4 were identified, whereas the linking M1 transitions were observed between the signature partners of the $\nu g_{7/2}$ band in the neighboring $^{119}$Xe [26] and $^{121}$Ba [27]. b) The signature splittings between bands 3 and 4 are very apparent, while almost no signature splittings were observed in the $\nu g_{7/2}$ bands of $^{119}$Xe and $^{121}$Ba. Band 3 even becomes energy favorable at $\hbar\omega > 0.32$ MeV. c) The most remarkable feature of band 3 is that it decays to the yrast $\nu h_{11/2}$ band via strong E1 transitions. In order to estimate the electric dipole strengths, B(E1) values were extracted for the E1 linking transitions between bands 3 and 2. They were obtained via the following expressions:

$$\frac{B(E1; I \to I-1)}{B(E2; I \to I-2)} = \frac{1}{1.3 \times 10^6} \frac{E_\gamma^5(E2)}{E_\gamma^3(E1)} \frac{I_\gamma(E1)}{I_\gamma(E2)} fm^{-2} \quad (5)$$

where the $\gamma$-ray energies are in MeV, $I_\gamma$(E1;I→I-1)/$I_\gamma$(E2;I→I-2) are the branching ratios of the decays from the states in band 3, and

$$B(E2; I \to I-2) = \frac{5}{16\pi} Q_0^2 \langle IK_i 20 \mid I-2K_f\rangle^2 \quad (6)$$

In (6), $Q_0 = 315$ efm was used, which was obtained from the shape parameter of $\beta_2 = 0.23$ predicted for the B configuration of $^{117}$Xe. The branching ratios were obtained from the spectra gated above the decaying levels. The deduced B(E1) values and the corresponding intrinsic dipole moments extracted via the rotational formula [28]:

$$B(E1; I \to I-1) = \frac{3}{4\pi} D_0^2 \langle IK_i 10 \mid I-1K_f\rangle^2 \quad (7)$$

are given in Table 2 together with the B(E1) value of the 205 keV ($7/2^- \to 5/2^+$) transition, which was obtained from the present half-life measurements.

It is well known that the E1 matrix elements between close-lying Nilsson orbitals are invariably small. The B(E1) is typically of the order of $10^{-6} \sim 10^{-5}$ Weisskopf unit (W.u.), e.g., the B(E1) value of the 205 keV ($7/2^- \to 5/2^+$) transition is $2\times10^{-6}$ W.u.. The B(E1) values of the transitions between bands 3 and 2 are much larger, of the order of $10^{-4}$ W.u., similar to that of the $5^- \to 6^+$ enhanced E1 transition observed in $^{114}$Xe. They also show an increase with spin as observed in $^{110}$Te at high spins [11] and the highest-lying E1 transition is enhanced by a factor of 100 comparing with the 205 keV transition. Such enhanced E1 transitions are considered as the most prominent experimental feature pointing to the existence of octupole correlations in this region [8]. Similar enhanced E1 transitions have also been observed very recently in $^{118}$Xe, $^{120}$Xe [12] and $^{121}$Xe [13]. These results unambiguously show the occurrence of octupole correlations in these isotopes. Cottle et al. investigated the systematics of the $5^-$ and $7^-$ states of the negative-parity bands observed in the even-xenon isotopes near N=66, and drew a conclusion that the behavior of $5^-$ and $7^-$ states of most of the lighter ($N \leq 72$) Te, Xe and Ba isotopes is consistent with an octupole origin [29]. These new experimental results are likely to support it.

However, according to the existing theoretical studies, no octupole deformation or softness is expected for the ground states in nuclei with N=63-67 in this region [7,8], though the responsible $d_{5/2}$ and $h_{11/2}$ orbitals are close to each other near the Fermi surface. Analogous situations have been observed in heavier lanthanide nuclei [30]. In $^{163}$Er, for example, which is well quadrupolly deformed and stable against octupole instability in the ground state, a similar set of enhanced E1 transitions [31] was observed. Theoretical calculations using the macroscopic-microscopic method have predicted that octupole correlations will occur for these Z≈70, N≈96 nuclei at medium spins [30]. The effect of rotation on the octupole instability in our considered region should be checked using a similar method. Noting that the A∼120 nuclei are $\gamma-$soft, the triaxial degree of freedom should be considered in the calculations, but this will make the theoretical study very difficult [32]. The low-spin states of the decoupled negative-parity bands in $^{118,120}$Xe are suggested to have an octupole vibrational character [12, 29]. In the neighboring odd-A isotopes, the close $d_{5/2}$ and $h_{11/2}$ states are expected to become mixed by the coupling to the octupole vibration. Therefore enhanced E1 transitions would be more favorably detected than in their even neighbors. And in fact, more enhanced E1 transitions have been observed in $^{117,121}$Xe than in $^{118,120}$Xe. Similar conclusion has been obtained for the lighter nuclei around $^{112}$Ba from calculations [8].

In this region, the pure spherical states $\nu g_{7/2}$ and $\nu d_{5/2}$ are mixed together when nuclei are quadrupolly deformed. The uniqueness of band 3 of $^{117}$Xe likely originates from the large component of $d_{5/2}$ in its configuration, the oc-

**Table 2.** Observed dipole strengths in $^{117,118,120,121}$Xe

| nuclide | $I_i^\pi \to I_f^\pi$ | B(E1)/B(E2) ($10^{-7}$fm$^{-2}$) | B(E1) ($10^{-4}$e$^2$fm$^2$) | B(E1) ($10^{-4}$W.u.) | $\|D_0\|$ (efm) |
|---|---|---|---|---|---|
| $^{117}$Xe | $\frac{7}{2}^- \to \frac{5}{2}^+$ | | $3.00 \times 10^{-2}$ | $2.00\times10^{-2}$ | |
| | $\frac{13}{2}^+ \to \frac{11}{2}^-$ | 0.255 | 0.54 | 0.35 | 0.024 |
| | $\frac{17}{2}^+ \to \frac{15}{2}^-$ | 0.305 | 0.81 | 0.53 | 0.028 |
| | $\frac{21}{2}^+ \to \frac{19}{2}^-$ | 0.457 | 1.35 | 0.90 | 0.035 |
| | $\frac{25}{2}^+ \to \frac{23}{2}^-$ | 0.654 | 2.04 | 1.36 | 0.043 |
| | $\frac{29}{2}^+ \to \frac{27}{2}^-$ | 1.06 | 3.43 | 2.29 | 0.055 |
| $^{121}$Xe [13] | $\frac{23}{2}^+ \to \frac{21}{2}^-$ | | 0.13 | | |
| | $\frac{11}{2}^+ \to \frac{9}{2}^-$ | | 0.29 | | |
| | $\frac{15}{2}^+ \to \frac{13}{2}^-$ | | 1.0 | | |
| | $\frac{19}{2}^- \to \frac{17}{2}^+$ | | 1.8 | | |
| | $\frac{21}{2}^+ \to \frac{19}{2}^-$ | | 2.6 | | |
| | $\frac{25}{2}^+ \to \frac{23}{2}^-$ | | 4.2 | | |
| $^{118,120}$Xe [12] | $9^- \to 8^+$ | | 2∼3 | | |
| | $7^- \to 6^+$ | | 2∼3 | | |
| | $8^- \to 8^+$ | | 2∼3 | | |

tupole interaction between $d_{5/2}$ and $h_{11/2}$ may lower the intrinsic excitation energy of band 3.

### 5.4 Band 5

Band 5 is a strongly coupled, positive-parity band and seems to be built directly on the ground state, i.e., the $\nu d_{5/2}$ K=5/2 orbital. The experimental B(M1)/B(E2) ratios for this band have been extracted from the coincidence data using the approximate expression

$$\frac{B(M1;I\to I-1)}{B(E2;I\to I-2)} = 0.693\frac{E_\gamma^5(E2)}{E_\gamma^3(M1)}\frac{I_\gamma(M1)}{I_\gamma(E2)}(\frac{\mu_N}{eb})^2 \quad (8)$$

Where the $\gamma$-ray energies are in MeV, and the E2/M1 mixing ratios $\delta$ for the $\Delta$I=1 transitions have been neglected. Theoretical estimates for the B(M1)/B(E2) ratios can be obtained from the formula based on the geometrical model of Dönau and Frauendorf [33]

$$\begin{aligned}\frac{B(M1;I\to I-1)}{B(E2;I\to I-2)} &= \frac{12}{5Q_0^2\cos^2(30^\circ+\gamma)} \\ &\times[1-\frac{K^2}{(I-1/2)^2}]^{-2}\frac{K^2}{I^2} \\ &\times\{(g_1-g_R)[(I^2-K^2)^{1/2}-i_1]-(g_2-g_R)i_2\}^2(\frac{\mu_N}{eb})^2\end{aligned} \quad (9)$$

$Q_0$ is the intrinsic quadrupole moment, $g_R$ is the gyromagnetic factor for a rotating core and is approximated by Z/A, $g_1$ the factor for the single quasiparticle excitation, and $g_2$ for the aligning quasiparticle in a band crossing. The last term is omitted since the experimental data are from below the bandcrossing. The theoretical estimates were calculated for the positive-parity [402]5/2$^+$, [411]3/2$^+$ and [413]5/2$^+$ configurations. The $g_1$[34] and $i_1$parameters used in the calculations are summarized in Table 3. Similar deformations were assumed for these configurations; i.e. $\beta_2 \sim 0.235$ and $\gamma \sim -10^\circ$, estimated for the lowest positive-parity configurations from the TRS calculations, were adopted in the calculations. The experimental values lie between the theoretical curves of the K=5/2 and 3/2 $\nu d_{5/2}$ orbitals (see Fig. 6), indicating the mixture of the two orbitals in the intrinsic structure of band 5. At low rotational frequencies the theoretical estimate reproduce the experimental data points better for K=5/2 than for K=3/2. With increasing rotational frequency the wave functions are expected to become more and more mixed which results in a lowering of the effective K-value for this $d_{5/2}$ band. Though a smaller $\beta_2(\sim 0.15)$, suggested for the [402]5/2$^+$ configuration in [12], will increase a little the corresponding theoretical B(M1)/B(E2) branching ratios. A value of $\delta \neq 0$ will reduce the experimental values. However, no reasonable deformation change or non-zero mixing ratios in band 5 will in substantial way change the implications of Fig. 6.

**Table 3.** Parameters used to calculate the B(M1)/B(E2) ratios

| Configuration | g-factor | K-value | $i_x$ |
|---|---|---|---|
| $\nu d_{5/2}$ | -0.33 | 2.5 | 0.5 |
| | -0.33 | 1.5 | 1.5 |
| $\nu g_{7/2}$ | -0.21 | 2.5 | 1.5 |

The angular momentum alignments of band 5 show a clear increase at the top, indicating a bandcrossing at $\hbar\omega \approx 0.34$ MeV, which is also attributed to the alignment of a pair of $\nu h_{11/2}$ neutrons (EF). This critical frequency support a similar $\beta_2$ for bands 3, 4 and 5, since the neutron $(h_{11/2})^2$ alignment frequency depends sensitively on the quadrupole deformation [35].

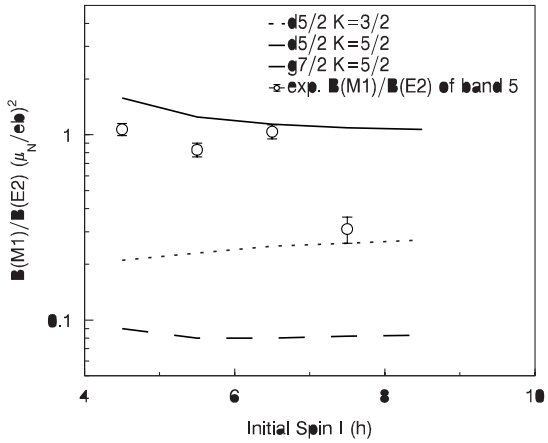


**Fig. 6.** Experimental $\frac{B(M1;I\rightarrow I-1)}{B(E2;I\rightarrow I-2)}$ ratios for band 5, the lines are model predictions

Level sequence 6 is a typical non-collective excitation structure. The origin of this structure is still unclear. Due to the lack of the assignments of the spins and parities of its levels, no configuration information can be deduced for these states.

## 6 Summary

Rotational bands in $^{117}$Xe have been studied by means of in-beam spectroscopic techniques. A positive-parity band (band 3) was observed for the first time, it decays to the $\nu h_{11/2}$ band (band 2) via five enhanced E1 transitions. Together with the recent observation of the similar enhanced E1 transitions in $^{118,120,121}$Xe, the occurrence of octupole correlations in nuclei with Z≈56, N≈64 is definitely determined, which contradicts the known theoretical calculations. More and systematic experimental results on the octupole collectivity in this mass region are still needed and new theoretical studies are requested. The known $\nu h_{11/2}$ and $\nu g_{7/2}$ bands have been extended up to high spins, and the experimentally observed bandcrossings are well interpreted with the TRS and CSM calculations. The measured B(M1)/B(E2) ratios support the $\nu d_{5/2}$ $[402]5/2^+$ assignment for the strongly coupled positive-parity band (band 5). Half-lives of the $11/2^-$ and $7/2^-$ levels were determined to be 59±20 ns and 16.5± 8.0 ns, respectively.

This work is supported by the Chinese Academy of Sciences and the National Science Foundation of China. We are very grateful to Insitut für Kernphysik der Universität Köln and Dr. K. O. Zell for providing the $^{92}$Mo target.

## References

1. Y. Liang, D. B. Fossan, J. R. Hughes, D. R. LaFosse, T. Lauritsen, R. Ma, E. S. Paul, P. Vaska, M. P. Waring, and N. Xu, Phys. Rev. C **45**, 1041 (1992)
2. E. S. Paul, R. M. Clark, S. A. Forbest, D. B. Fossan, J. R. Hughes, D. R. LaFosse, Y. Liang, R. Ma, P. J. Nolan, P. H. Regan, P. Vaska, R. Wadsworth and M. P. Waring, J. Phys. G **18**, 837 (1992)
3. S. Juutinen, S. Törmänen, B. Cederwall, A. Johnson, R. Julin, S. Mitarai, J. Mukai, P. Ahonen, B. Fant, F. Liden, J. Nyberg and I. Ragnarsson, Z. Phys. A **338**, 365 (1991)
4. E. S. Paul, D. B. Fossan, K. Hauschild, I.M. Hibbert, H. Schnare, J. M. Sears, I. Torslund, R. Wadsworth, A. N. Wilson and J. N. Wilson, Phys. Rev. C **51**, R2857 (1995)
5. P. Möller and J. R. Nix, Nucl. Phys. **A361**, 117 (1981)
6. W. Nazarewicz, P. Olanders, I. Ragnarsson, J. Dudek, G. Leander, P. Möller and E Ruchowska, Nucl. Phys. **A429**, 269 (1984)
7. J. Skalski, Phys Lett. B **238,** 6 (1990)
8. P. -H. Heenen, J. Skalski, P. Bonche, and H. Flocard, Phys. Rev. C **50,** 802 (1994)
9. P. Möller and J. R. Nix, At. Data Nucl. Data Tables **29**, 402 (1988)
10. S. L. Rugari, R. H. France III, B. J. Lund, Z. Zhao, M. Gai, P. A. Butler, V. A. Holliday, A. N. James, G. D. Jones, R. J. Poynter, R. J. Tanner, K. L. Ying, and J. Simpson, Phys. Rev. C **48**, 2078 (1993)
11. E. S. Paul, H. R. Andrews, T. E. Drakes, J. DeGraaf, V. P. Janzen, S. Pilotte, D. C. Radford, and D. Ward, Phys. Rev. C **50**, R534 (1994)
12. S. Törmänen, S. Juutinen, R. Julin, B. Cederwall, A. Johnson, R. Wyss, P. Ahonen, B. Fant, M. Matsuzaki, J. Nyberg, M. Piiparinen, S. Mitarai, J. Mukai, and A. Virtanen, Nucl. Phys. **A572**, 417 (1994)
13. J. Timár, J. Simpson, E. S. Paul, S. Araddad, C. W. Beausang, M. A. Bentley, M. J. Joyce and J. F. Sharpey-Schafer, J. Phys. G **21**, 783 (1995)
14. P. Chowdhury, U. Garg, T. P. Sjoreen, and D. B. Fossan, Phys. Rev. C **23**, 733 (1981)
15. S. Törmänen, R. Julin, S. Juutinen, P. Ahonen, B. Cerdwall, A. Johnson, S. Mitarai, J. Mukai, and J. Nyberg, Nucl. Data Sheets **66**, 495 (1992)
16. G. Marguier, C. Richard-Serre, J. Genevey, M. Morgue, A. Charvet, J. Giroux, A. Huck, A. Knipper, and G. Walter, J. Phys. G **12**, 757 (1986)
17. Z. Liu, X. Sun, X. Zhou, X. Lei, Y. Zhang, H. Jin, Q. Pan, Y. Guo, X. Chen, Y. Luo, S. Wen, G. J. Yuan, G. S. Li, and C. X. Yang, in Slide report of the International workshop on Latest Topics in Nuclear Structure, Beijing, Oct. 1993, edited by Xu Jincheng, p60
18. Z. Liu, X. Sun, X. Zhou, X. Lei, Y. Zhang, H. Jin, Q. Pan, Y. Guo, X. Chen, Y. Luo, S. Wen, G. J. Yuan, G. S. Li, C. X. Yang, W. D. Luo, and Y. S. Chen, Nucl. Phys. **A583**, 221c (1995)
19. Z. Liu, X. Sun, X. Zhou, X. Lei, Y. Zhang, H. Jin, Q. PAn, Y. Guo, X. Chen, Y. Luo, S. Wen, G. J. Yuan, G. S. Li, C. X. Yang, W. D. Luo, and Y. S. Chen, Z. Phys. A **351**, 363 (1995)
20. V. Barci, J. Gizon, A. Gizon, J. Crawford, J. Genevey A. Plochocki and M. A. Cunningham, Nucl. Phys. **A383**, 309 (1982)
21. S. Ohya, T. Tamura, Nucl. Data Sheets **60**, 600 (1993)
22. Liu Zhong, Sun Xiangfu, Guo Yingxiang, Lei Xiangguo, Chen Xinfeng, Zhou Xiaohong, Zhang Yuhu, Jin Hanjuan, Luo Yixiao, Wen Shuxian, Yuan Guanjun, Li Guangsheng, Yang Chunxiang, and Liu Xiangan, to be published in High Energy Phys. and Nucl. Phys., 1997 (in Chinese)

23. K. S. Krane, R. M. Steffen, and R. M. Wheeler,Nucl. Data Tables A **11**, 351 (1973)
24. M. Gai, D. M. Gordon, R. E. Shroy, and D. B. Fossan, Phys. Rev. C **26**, 1101 (1982)
25. R. Bengtsson, and S. Frauendorf, Nucl. Phys. **A327**, 139 (1979)
26. V. P. Janzen, M. P. Carpenter, L. L. Riedinger, W. Schmitz, D. G. Popescu, J. A. Cameron, J. K. Johansson, D. D. Rajnauth, J. C. Waddington, G. Kajrys, S. Monaro, and S. Pilotte, Phys. Rev. C **39**, 2050 (1989)
27. B. Cederwall, A. Johnson, R. Wyss, C. G. Linden, S. Mitarai, J. Mukai, B. Fant, S. Juutinen, P. Ahonen and J. Nyberg, Nucl. Phys. **A529**, 410 (1991)
28. P. A. Butler,and W. Nazarewicz, Nucl. Phys. **A533**, 249 (1991)
29. P. D. Cottle, K. A. Stuckey, and K.W. Kemper, Phys. Lett. **B 219**, 27 (1989)
30. P. A. Butler, in Proceedings of the International Conference on High-Spin Physics and Gamma-Soft Nuclei, Pittsburgh, 1990, edited by J. X. Saladin and R. Sorensen (World Scientific, Singapore, 1991), p. 552
31. J. C. Bacelar, M. Diebel, O. Andersen, J. D. Garrett, G. B. Hagemann, B. Herskind, J. Kownacki, C. X. Yang, L. Carlen, J. Lyttkens, H. Ryde, W. Walus and P. O. Tjøm, Phys. Lett. **B 152**, 157 (1985)
32. W. Nazarewicz, Nucl. Phys. **A520**, 333c (1990)
33. F. Dönau and S. Frauendorf, in Proceedings of the Conference on High Angular Momentum Properties of Nuclei, Oak Ridge, 1982, edited by N. R. Johnson (Harwood Academic, New York, 1983), p.143
34. T. Lönnroth, S. Vajda, O. C. Kistner and M. H. Rafailovich, Z. Phys. A **317**, 215 (1984)
35. R. Wyss, A. Granderath, R. Bengttson, P. Von. Brentano, A. Dewald, A. Gelberg, A. DGizon, J. Gizon, S. Harrisspulos, A. Johnson, W. Lieberz, W. Nazarewicz, J. Nyberg and K. Shiffer, Nucl. Phys. **A505** 337 (1989)